Estimation of variance distribution in three-dimensional reconstruction. I. Theory

Weiping Liu*

Wadsworth Center, New York State Department of Health, Albany, New York 12201-0509, and Department of Physics, University of New York at Albany, Albany, New York 12222

Joachim Frank

Wadsworth Center, New York State Department of Health, Albany, New York 12201-0509, and Department of Biomedical Sciences, University of New York at Albany, Albany, New York 12222

Received March 9, 1995; accepted July 5, 1995

A theory is developed for estimating the three-dimensional (3-D) variance of a 3-D image reconstructed from projections by weighted backprojection. The theory is applicable for any data-collection schemes that produce partially redundant sampling of the angular space. The particular data collection considered here, the single-exposure random-conical scheme, is used for the reconstruction of macromolecules in electron microscopy. In this context, the purpose of the 3-D variance estimation is to detect and localize the conformational variability, to assess the significance of structural differences between two experimentally related 3-D images, and to assess the significance of local features in a 3-D image. The 3-D variance estimate of each reconstruction voxel is obtained by (i) the comparison of closest points on Fourier sections associated with difference projections, (ii) the comparison of neighbor projections in real space, or (iii) the comparison of projections with reprojections of the reconstruction.

1. INTRODUCTION

A. Rationale of the Three-Dimensional Variance Estimation

Within the past twenty years, three-dimensional (3-D) imaging techniques by reconstruction from projections have found wide applications in many fields of science. The theoretical foundation for these techniques was developed by Radon[1] and Cormack.[2] The 3-D visualization of biological objects by electron microscopy has become an important tool of structural biology, starting with the pioneering work in reconstructing the helical T4 phage tail from its projection.[3] In essence, the transmission electron microscope produces a projection of the object, which is recorded as an image on the photographic plate. The physical quantity whose projection is recorded is the object's Coulomb potential distribution.[4] Through the application of 3-D reconstruction techniques, a 3-D image of the object can be formed when a sufficient number of projections covering the angular space are available.

There are two categories of biological objects: (i) ordered objects (e.g., aggregations of molecules with a repeating motif), which include helical structures,[3] particles with icosahedral symmetry,[5] and two-dimensional (2-D) crystals[6]; and (ii) unordered objects, which include subcellular structures[7] embedded in plastic and single macromolecules.[8] In electron microscopy of biological objects, the resolution is limited by the degree of order for ordered specimen, level of specimen preservation, and radiation damage of specimen under an electron beam. For ordered objects, their repeating motif permits a very low electron dose to be used and, potentially, atomic resolution to be achieved. For subcellular structures, on the other hand, a large number of projections have to be collected from the same structure, and the attainable resolution is limited by the radiation damage.[7] The situation with single macromolecules falls between the above two extremes, as is explained below.

In this paper we deal specifically with techniques for 3-D reconstruction of macromolecules that exist in single-particle form. For such objects, the angular space is covered when the specimen grid supporting the macromolecule is tilted, when preexisting orientations of the macromolecule are used, or by a combination of both. Because of the extreme radiation sensitivity of macromolecules, any data-collection technique that requires collection of multiple views from the same specimen is unacceptable. (The only exception is the technique of automated tomography, which requires a specialized computer-controlled instrument.) This realization has led to the development of reconstruction methods that exploit the fact that the molecule is available in hundreds or thousands of copies with identical structures.

One of these methods, the so-called random-conical reconstruction method,[9,10] has been used successfully to produce 3-D images of macromolecular assemblies, such as ribosomes,[11] hemocyanin,[12] and calcium release channel,[13] that could not be obtained in a crystalline form amenable to x-ray crystallographic study. More recently, the extension of the random-conical method to single macromolecules embedded in ice[14,15] has opened up the prospect of a quantitative structure determination of such molecules with the electron microscope. Especially intriguing is the possibility of locating binding sites of ligands in three dimensions. Examples of successful localizations are the 40S mammalian ribosomal

0740-3232/95/122615-13$06.00

subunit-eIF-3 complex[16] and the *Androctonus australis* hemocyanin-Fab immunocomplex.[17,18]

The large amount of noise in the individual projections [signal-to-noise ratios (SNR's) are normally in the range of 1] that propagates to the 3-D image raises questions about the reproducibility of individual features in this image. For different experiments, these questions arise in different forms: after reconstructing a macromolecule, we wish to know whether a given feature is significant or merely the result of a statistical fluctuation. In a ligand-binding experiment or in an experiment that may involve a conformational change, there is the need to compare two 3-D maps and to interpret the resulting 3-D difference map. Here the question is, which of the difference peaks represent significant physical changes and which should be discounted as being likely due to statistical fluctuations?

We address these questions in our investigation by using the 3-D variance, which can be estimated from the random-conical projection data for any linear reconstruction algorithm. The purpose of the 3-D variance analysis is to assess the significance of structural differences of two related reconstructions, to assess the significance of local features in a reconstruction, and to detect 3-D conformational changes. A brief account of this work has been given elsewhere.[19,20]

B. Random-Conical Data-Collection and Reconstruction Method

The single-exposure random-conical reconstruction method[9,10,21] takes advantage of the fact that macromolecules often have one or several preferred orientations of the specimen grid. A specimen field that contains a number of molecules is imaged twice: first with the specimen tilted to a maximum tilt angle (e.g., 50°) and subsequently with the specimen in an untilted position. After digitization of the electron micrographs, the tilted and the untilted projections of each molecule are selected simultaneously on the computer screen. The tilted projections, by virtue of the random azimuthal orientations of the molecules on the specimen grid, form a random-conical set that can be used to reconstruct the molecule in three dimensions (Fig. 1). The purpose of the untilted projections is threefold: (i) to determine the precise azimuth of each molecule and thereby the azimuth of the corresponding tilted projection in the conical geometry, (ii) to divide the molecules into homogeneous groups according to their appearance in this view[22] (classification), and (iii) to obtain an average for each group that can serve as a control of the reconstruction procedure (self-consistency test).

In summary, the typical reconstruction procedure involves the following steps:

1. Recording of two electron micrographs from the same specimen field (tilted and untilted);
2. Simultaneous extraction of molecules from the tilted- and the untilted-specimen projections;
3. Alignment and classification of untilted-specimen projections;
4. Alignment of tilted-specimen projections;
5. Weighted backprojection reconstruction from the tilted-specimen projections;
6. Visualization of the results by the use of surface and volume rendering.

To this protocol we now add another important step:

7. Computation of the 3-D variance estimate and analysis of the 3-D map in the light of this result.

C. Projection-Noise Sources

For data from a single-exposure random-conical tilt series, the projection-noise sources can be categorized in the following way:

1. Variations of particle structures on the grid:

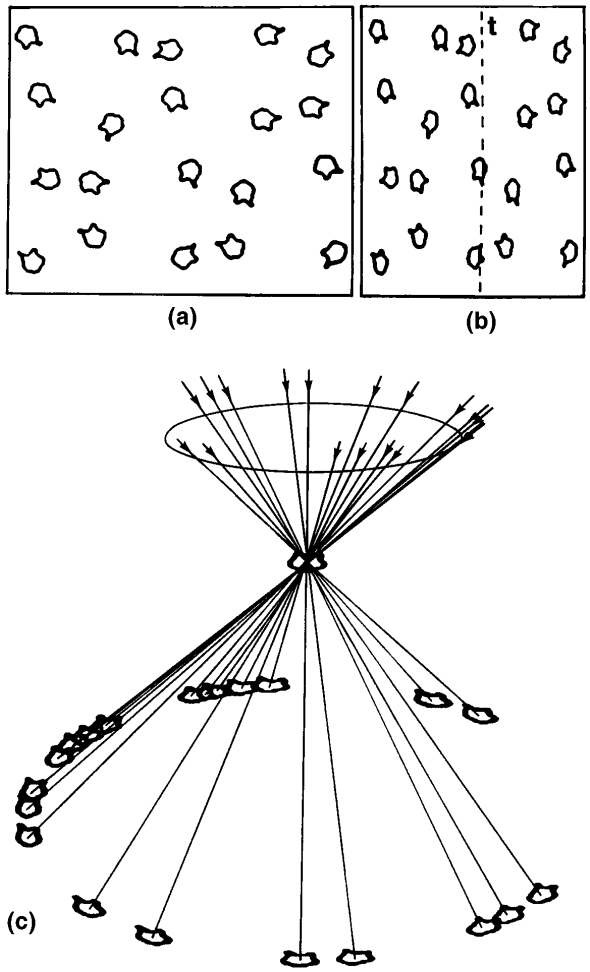

Fig. 1. Data-collection scheme of a single-exposure random-conical tilt series: (a) specimen with particles in the same in-plane orientation and with random azimuthal angles; (b) the same specimen tilted by a high angle, 45°–60°. First an image of tilted specimen (b) is recorded. An image of untilted specimen (a) is taken subsequently. With the azimuthal angle determined from the untilted view and the tilt angle derived by the use of the particles as markers, each particle selected from tilted image (b) can be arranged in its appropriate place in a conical tilt series (c). Three features of this data-collection scheme are worth noting: (i) the azimuthal angles of the projections in a data set are randomly distributed over 360°, (ii) each view angle has only one projection, and (iii) experimentally we can collect as many projections as we desire; hence most projections have at least one neighbor with a closely neighbored view angle. (Reproduced from Ref. 10 with permission by Blackwell Scientific Publishers.)

- Variations that are due to the coexistence of different conformational states, such as waving of a bound antibody around its binding site, opening and closing of channels, etc.
- Variations in the distribution of stain.
- Carbon film noise that is due to the variations of the amorphous carbon film structure.
- Structural changes that are due to radiation damage, which can be reduced by the use of low exposure.
- Misalignment of projections, which can be considered as small random rotations and translations of the particles.

2. Structure-related instrumental-noise sources:

- Quantum noise from elastically scattered electrons that form the bright field image.
- Quantum noise from inelastically scattered electrons that form a low-resolution background image.
- Photographic film noise.

3. Noise related to sampling:

- Microdensitometer noise.
- Interpolation errors.

Resolution-limiting factors that cannot be removed by the use of redundant information are stain variation, conformational changes, and related misalignment. Stain variation limits the ultimate resolution to 15–20 Å, which is well below the resolution of the instrument (2–3 Å). (0.1 Å=1 nm).

D. Context and Strategy of Variance Estimation

The 3-D variance analysis, in essence, is a special case of a general statistical estimation problem, with the estimator being the variance of a multivariate statistical function. In our case, the multivariate function is the 3-D image of an object, obtained by reconstruction, and the statistical variables are the measured samples of the projections.

Variance information is tractable to different extents in different fields of biological imaging. In x-ray crystallography, the conformational heterogeneity in protein crystals is averaged out in the diffraction pattern, and it is difficult to obtain detailed information without the use of stereochemical data in the refinement step.[23] In positron emission tomography the effects of accidental and scatter coincidences, dead-time losses, and attenuation of the annihilation photons on the reconstruction are analyzed by the use of the tools of statistics.[24] In nuclear magnetic resonance spectroscopy[25,26] the experimental nuclear magnetic resonance spectrum is a reflection of average conformational states of the molecule in solution that define the possible conformational space that agrees with the experimental data and constraints. The structural variability of the molecule is studied by the comparison of a number of possible conformations that are obtained from searching the conformational space repeatedly.[25]

In electron microscopy, the problem of quantum noise propagation from projections to the 3-D image has been discussed by Hegerl and Hoppe.[27] In this paper a 3-D variance estimation algorithm is developed that is valid for any weighted backprojection (or any linear shift-invariant) reconstruction method. In contrast to Hegerl and Hoppe's treatment,[27] in which the variance was also derived for a true 3-D reconstruction problem, we do not have to assume independence of noise among pixels of the same projection.

From the outset, we must distinguish two types of 3-D variance involved in this paper, which we define by appropriate "gedankenexperiments":

Type I: Let us assume that, in a given actual experiment, exactly N projections that present N viewing directions are found. We now define an associated gedankenexperiment in the following way: for each of these viewing directions, a large set (say, M) of projections is measured. From these $N \times M$ projections, we can compute M independent reconstructions. The type-I variance is defined by a voxelwise comparison of these reconstructions; it is a measure of the reliability of the actual 3-D reconstruction. Note that, because of the properties of the random-conical data collection, multiple measurement of projections at each angle is in reality not possible because each tilted–untilted micrograph pair yields a different set of view angles and each projection corresponds to a different particle on the grid.

Type II: For each particle, it is assumed that an entire set of projections is available, enough to reconstruct it unambiguously. It would then be possible, following this new gedankenexperiment, to reconstruct each particle and then proceed to form the average particle and its variance. This type-II variance can describe the 3-D particle conformational changes.

We show that the random-conical data-collection scheme permits the type-I, but not type-II, variance to be estimated. However the type-II variance is also discussed because it provides a conceptional reference. The main focus of this paper is on the type-I variance, and this is what the term 3-D variance implies in the remainder of the paper.

Based on the 3-D variance's definition and the tracing of the noise contributions along the route of reconstruction, a theoretical relationship between the 2-D variances of the projections and the 3-D variance of the reconstruction is first established. From noise information hidden in the redundant number of projections (in which the term redundant is relative to Shannon's sampling requirement in 3-D Fourier space), noise levels of each projection can then be estimated in three different ways: (i) by a comparison of the closest points among the projection data in 3-D Fourier space (applicable to arbitrary projection geometries but computationally demanding), (ii) by a comparison of neighboring projections in real space (computationally economical but quite restrictive; each projection has to have at least one neighbor), or (iii) by a comparison of a projection and its corresponding reprojection from the reconstruction (subject to a certain systematic error). The 3-D variance estimate is subsequently calculated from the projection-noise estimates.

2. THEORY OF THREE-DIMENSIONAL VARIANCE ESTIMATION

A. Relationship between Three-Dimensional Variance and Projection Variances

In the formal presentation of the problem, we make use of the following notational conventions: (1) A function

in real space is represented by a lowercase letter, and its Fourier transform is represented by the corresponding capital letter; (2) 3-D coordinates are denoted by capital letters, and 2-D coordinates are denoted by lowercase letters; (3) in the operation between the Fourier transform of a 2-D projection and a 3-D function in Fourier space, the former is implied to be lying in a central plane in 3-D Fourier space oriented according to the projection's viewing direction; (4) a sampled function, for example $p^{(i)}(k, l)$, when convoluted with a continuous function, is understood to mean $\sum_{k,l} p^{(i)}(k, l)\delta[\mathbf{r} - (k, l)]$; (5) in all derivations, the projection sampling rate for (k, l) is defined to be 1. A consequence of this convention is that if the projection sampling rate as measured in the specimen space is T, the real-space coordinates will have the unit of T, and the Fourier-space coordinates will have the unit of $1/T$.

Furthermore, the following definitions apply: roman letters denote operations. Specifically, var( ) represents the operation of taking the ensemble variance; BP( ) means to backproject a 2-D projection into 3-D space; hence the result of BP( ) is a 3-D function; PJ_i denotes a projection operation in a direction denoted by i; $p^{(i)}(k, l)$ is the digitized, aligned projection indexed i; $W^{(i)}(\mathbf{u})$ is the weighting function for projection i; $W(\mathbf{U}) \equiv \sum_{i=1}^{N} W^{(i)}(\mathbf{u})$ is a 3-D weighting function; $f(\mathbf{R})$ is the 3-D low-pass filtration point-spread function (PSF) with the cutoff frequency U_f; U_f is an adjustable parameter, and its physical meaning is discussed in Section 5. Henceforth the term filtration is always used to mean low-pass filtration; and $f^{(i)}(\mathbf{r}) \equiv \mathrm{PJ}_i[f(\mathbf{R})]$ is the low-pass filtration PSF for projection i.

We first define the average projection and the average reconstruction (and from those the projection noise and the reconstruction noise) on the basis of the gedankenexperiment: we assume that we can measure M versions of a projection set with N fixed-view angles, or a total of $N \times M$ projections of $N \times M$ different versions of the molecule. (In reality this is impossible because each cast of N molecules will realize a different set of azimuthal angles; hence the gedankenexperiment must be used to define the concept of the relevant statistical quantities.)

The mth version of the experimental projection is $p_m^{(i)}(k, l)$. The corresponding reconstruction $b_m(\mathbf{R})$ is computed from the N projections at N view angles $\{p_m^{(i)};\ i = 1, \ldots, N\}$. The average projection i is defined as

$$\overline{p^{(i)}(k, l)} \equiv \lim_{M\to\infty}\left[\frac{1}{M}\sum_{m=1}^{M} p_m^{(i)}(k, l)\right],$$

and the average reconstruction is defined as

$$\overline{b^{(i)}(\mathbf{R})} \equiv \lim_{M\to\infty}\left[\frac{1}{M}\sum_{m=1}^{M} b_m^{(i)}(\mathbf{R})\right].$$

From now on, a overbar over an function always denotes the ensemble average from the above gedankenexperiment. Because for the random-conical tilt series, only one projection set is obtained (i.e., only one of the m's is realized), the trial index m can be ignored. For example, it is always implied that $p^{(i)}(k, l) = p_m^{(i)}(k, l)$ and $b(\mathbf{R}) = b_m(\mathbf{R})$.

Because of the large number of projections used in the reconstruction from a random-conical tilt series, the weighted backprojection method (which is characterized by computational efficiency, stability under noise, and mathematical tractability) has so far been the practical choice. Two similar types of weighting function have been proposed for arbitrary projection geometry.[28,29] Because of the linear property of the reconstruction, the weighting function can be applied individually to either the Fourier transforms of the projections or to the 3-D Fourier transforms of the unweighted backprojection.

Below we derive the variance of the weighted backprojection reconstruction as a function of projection noise under the condition that the projection-noise components from different view angles are independent. This is true for the random-conical data collection because projections from different view angles are collected from different particles. [In contrast, independence of noise components does not hold for a projection set obtained when a single particle is tilted into a number of orientations. In this case, the noise sources associated with the structural variations of the particle as listed in category (1) in Subsection 1.C are no longer independent among the projections.]

The linear interpolation process can be described by a convolution with an interpolation function $i(\mathbf{r})$:

$$p^{(i)}(\mathbf{r}) \equiv p^{(i)}(k, l) \otimes i(\mathbf{r}), \tag{2.1}$$

where $\otimes$ denotes the operation of 2-D convolution.

For bilinear interpolation,

$$i(\mathbf{r}) = \begin{cases} (1 - |x|)(1 - |y|) & \text{when } |x| \le 1 \text{ and } |y| \le 1 \\ 0 & \text{when } |x| > 1 \text{ or } |y| > 1 \end{cases}. \tag{2.2}$$

The 3-D reconstruction is

$$\begin{aligned} b(\mathbf{R}) &\equiv \left\{\sum_{i=1}^{N} \mathrm{BP}[\,p^{(i)}(\mathbf{r})]\right\} \otimes w(\mathbf{R}) \otimes f(\mathbf{R}) \\ &= \sum_{i=1}^{N} \mathrm{BP}[\,p_{wf}^{(i)}(\mathbf{r})]. \end{aligned} \tag{2.3}$$

We define the weighted and filtered projection as

$$\begin{aligned} p_{wf}^{(i)} &\equiv p^{(i)}(\mathbf{r}) \otimes w^{(i)}(\mathbf{r}) \otimes f^{(i)}(\mathbf{r}) \\ &= p^{(i)}(k, l) \otimes h_{iwf}^{(i)}(\mathbf{r}), \end{aligned} \tag{2.4}$$

in which the PSF is associated with interpolation, weighting, and filtration:

$$h_{iwf}^{(i)}(\mathbf{r}) \equiv i(\mathbf{r}) \otimes w^{(i)}(\mathbf{r}) \otimes f^{(i)}(\mathbf{r}). \tag{2.5}$$

Now we define the projection noise:

$$n^{(i)}(\mathbf{r}) \equiv p^{(i)}(\mathbf{r}) - \overline{p^{(i)}(\mathbf{r})}. \tag{2.6}$$

So from Eqs. (2.4) and (2.6), the weighted and filtered projection noise is

$$\begin{aligned} n_{wf}^{(i)}(\mathbf{r}) &\equiv p_{wf}^{(i)}(\mathbf{r}) - \overline{p_{wf}^{(i)}(\mathbf{r})} \\ &= n^{(i)}(k, l) \otimes h_{iwf}^{(i)}(\mathbf{r}). \end{aligned} \tag{2.7}$$

Because different projections come from different particles on the specimen grid, the projection-noise contributions are statistically independent, that is, $n^{(i)}(k, l)$ and $n_{wf}^{(i)}(\mathbf{r})$ are independent for different i's. From Eqs. (2.3) and (2.7), the 3-D variance is

$$\begin{aligned}\nu(\mathbf{R}) &\equiv \overline{[b(\mathbf{R}) - \overline{b(\mathbf{R})}]^2} \\ &= \sum_{i=1}^{N} \overline{\{\mathrm{BP}[n_{wf}^{(i)}(\mathbf{r})]\}^2} + \sum_{\substack{i,j=1 \\ i\neq j}}^{N} \overline{\mathrm{BP}[n_{wf}^{(i)}(\mathbf{r})]\mathrm{BP}[n_{wf}^{(j)}(\mathbf{r})]} \\ &= \sum_{i=1}^{N} \mathrm{BP}\overline{[n_{wf}^{(i)}(\mathbf{r})]^2} + \sum_{\substack{i,j=1 \\ i\neq j}}^{N} \mathrm{BP}\overline{[n_{wf}^{(i)}(\mathbf{r})n_{wf}^{(j)}(\mathbf{r})]} \\ &= \sum_{i=1}^{N} \mathrm{BP}[V_{wf}^{(i)}(\mathbf{r})], \end{aligned} \tag{2.8}$$

where

$$\nu_{wf}^{(i)}(\mathbf{r}) \equiv \overline{[n_{wf}^{(i)}(\mathbf{r})]^2}. \tag{2.9}$$

So we have obtained the important result that the 3-D variance is the sum of the backprojections of the weighted and filtered projection variances.

After deriving the 3-D variance as the function of projection variances, by utilizing the independence of the noise components among projections, we are now able to establish the 3-D variance estimate by means of the estimation of projection variances.

B. Estimation of Projection Variance For a Set of Projections with Arbitrary Orientations: Fourier-Space Comparison

Because we are dealing with data collections without multiple independent measurements of projection, we have to borrow measures from other projections to estimate the projection variance of this view angle. This procedure utilizes the information from the given redundant number of projections.

In this subsection, we estimate the 3-D variance for a projection set with arbitrary orientations by means of the comparison of projections in 3-D Fourier space.

The projection-noise component, written in terms of its Fourier transform, is

$$n_{wf}^{(i)}(\mathbf{r}) = \int N_{wf}^{(i)}(\mathbf{u})\exp(i2\pi\mathbf{r}\mathbf{u})\mathrm{d}^2\mathbf{u}. \tag{2.10}$$

Hence the weighted and filtered projection variance is

$$\begin{aligned}\nu_{wf}^{(i)}(\mathbf{r}) &\equiv \overline{[n_{wf}^{(i)}(\mathbf{r})]^2} \\ &= \iint C_{wf}^{(i)}(\mathbf{u}', \mathbf{u}'')\exp[i2\pi\mathbf{r}(\mathbf{u}' + \mathbf{u}'')]\mathrm{d}^2\mathbf{u}'\mathrm{d}^2\mathbf{u}'', \end{aligned} \tag{2.11}$$

where the weighted and filtered spectral projection covariances

$$C_{wf}^{(i)}(\mathbf{u}', \mathbf{u}'') = C^{(i)}(\mathbf{u}', \mathbf{u}'')H_{iwf}^{(i)}(\mathbf{u}')H_{iwf}^{(i)}(\mathbf{u}''), \tag{2.12}$$

$$C^{(i)}(\mathbf{u}', \mathbf{u}'') \equiv \overline{N^{(i)}(\mathbf{u}')N^{(i)}(\mathbf{u}'')} \tag{2.13}$$

are the spectral projection covariances.

Thus, from the weighted, filtered spectral projection covariance, the projection variance in real space can be derived.

We now try to find a 3-D variance estimate from the above relationships. Let us assume that the distance between any two Fourier points in two projection transforms, $\mathbf{u}^{(i)}$ and $\mathbf{u}_s^{(j)}$, is small enough [namely, $|\mathbf{u}^{(i)} - \mathbf{u}_s^{(j)}| < 1/(3D)$, where D is the diameter of the object; see Appendix A] so that the signal components and noise statistics of $P^{(i)}(\mathbf{u})$ and $P^{(j)}(\mathbf{u}_s)$ are the same. We can estimate the spectral projection noise at $\mathbf{u}^{(i)}$:

$$\begin{aligned}\tilde{N}_j^{(i)}(\mathbf{u}) &= [P^{(i)}(\mathbf{u}) - P^{(j)}(\mathbf{u}_s)]/\sqrt{2} \\ &\approx [N^{(i)}(\mathbf{u}) - N^{(j)}(\mathbf{u}_s)]/\sqrt{2}. \end{aligned} \tag{2.14}$$

To minimize the error that is due to the projection signal component differences, we should search point $\mathbf{u}_s^{(j)}$ in such a way that it is the closest point to $\mathbf{u}^{(i)}$ from among all other $(N - 1)$ projection central section planes. If $\mathbf{u}^{(i)}$ is situated on a common line, these two points will coincide.

Now we assume that we have obtained noise component estimates for two Fourier points, $\mathbf{u}'$ and $\mathbf{u}''$, on projection i. We can then obtain the spectral covariance estimate between these two points:

$$\tilde{C}^{(i)}(\mathbf{u}', \mathbf{u}'') = \lambda_{jk}\tilde{N}_j^{(i)}(\mathbf{u}')\tilde{N}_k^{(i)}(\mathbf{u}''), \tag{2.15a}$$

where

$$\lambda_{jk} \equiv \begin{cases} 1 & \text{when } j = k \\ 2 & \text{when } j \neq k \end{cases}. \tag{2.15b}$$

Equation (2.15a) can be proved to be an unbiased estimate following the independence property of noise components among projections.

We have the 3-D variance estimate:

$$\tilde{\nu}(\mathbf{R}) = \sum_{i=1}^{N} \mathrm{BP}[\tilde{\nu}_{wf}^{(i)}(\mathbf{r})], \tag{2.16}$$

where

$$\begin{aligned}\tilde{\nu}_{wf}^{(i)}(\mathbf{r}) = \iint\ & \tilde{C}^{(i)}(\mathbf{u}', \mathbf{u}'')H_{iwf}^{(i)}(\mathbf{u}')H_{iwf}^{(i)}(\mathbf{u}') \\ & \times \exp[i2\pi\mathbf{r}\cdot(\mathbf{u}' + \mathbf{u}'')]\mathrm{d}^2\mathbf{u}'\mathrm{d}^2\mathbf{u}''. \end{aligned} \tag{2.17}$$

The direct implementation of Eq. (2.17) is computationally intensive because the spectral covariance estimate $\tilde{C}^{(i)}(\mathbf{u}', \mathbf{u}'')$ is a four-dimensional function. But because the projection data needed to compute $\tilde{\nu}_{wf}^{(i)}(\mathbf{r})$ of Eq. (2.17) are two dimensional, a better form of Eq. (2.17) should exist in terms of its practical computation. Such a form can be derived by analysis, either in Fourier or in real space, as shown below.

In the spectral-noise estimation from Eq. (2.14), the Fourier space of projection i is divided into $(N - 1)$ regions, with each region's corresponding to the comparison of projection i with a different projection. Let $S_j^{(i)}$ represent the Fourier region of projection i where projection j is compared. Then

$$p_{wf}^{(i)}(\mathbf{r}) = \sum_{\substack{j=1 \\ j\neq i}}^{N} p_{wfj}^{(i)}(\mathbf{r}), \tag{2.18}$$

where

$$p_{wfj}^{(i)}(\mathbf{r}) = \int_{u\subset S_j^{(i)}} P_{wf}^{(i)}(\mathbf{u})\exp(i2\pi\mathbf{r}\cdot\mathbf{u})\mathrm{d}^2\mathbf{u}\,. \tag{2.19}$$

The corresponding noise components have

$$\nu_{wf}^{(i)}(\mathbf{r}) = \sum_{\substack{j=1\\ j\neq i}}^{N}\sum_{\substack{k=1\\ k\neq i}}^{N} c_{wfjk}^{(i)}(\mathbf{r})\,, \tag{2.20}$$

where

$$c_{wfjk}^{(i)}(\mathbf{r}) \equiv \overline{n_{wfj}^{(i)}(\mathbf{r})n_{wfk}^{(i)}(\mathbf{r})}\,. \tag{2.21}$$

From these relationships, we can establish the corresponding 3-D variance estimate as

$$\tilde{c}_{wfjk}^{(i)}(\mathbf{r}) = \lambda_{jk}\tilde{n}_{wfj}^{(i)}(\mathbf{r})\tilde{n}_{wfk}^{(i)}(\mathbf{r})\,, \tag{2.22}$$

where

$$\tilde{n}_{wfj}^{(i)}(\mathbf{r}) = \int_{u\subset S_j^{(i)}} \tilde{N}^{(i)}(\mathbf{u})H_{iwf}^{(i)}(\mathbf{u})\exp(i2\pi\mathbf{r}\cdot\mathbf{u})\mathrm{d}^2\mathbf{u}\,, \tag{2.23}$$

and $\tilde{N}^{(i)}(\mathbf{u})$ is from Eq. (2.14).

So

$$\begin{aligned}\tilde{\nu}_{wf}^{(i)}(\mathbf{r}) &= \sum_{\substack{j=1\\ j\neq i}}^{N}\sum_{\substack{k=1\\ k\neq i}}^{N} \tilde{c}_{wfjk}^{(i)}(\mathbf{r})\\ &= 2[\tilde{n}_{wf}^{(i)}(\mathbf{r})]^2 - \sum_{\substack{j=1\\ j\neq i}}^{N}[\tilde{n}_{wfj}^{(i)}(\mathbf{r})]^2,\end{aligned} \tag{2.24}$$

where

$$\tilde{n}_{wf}^{(i)}(\mathbf{r}) = \tilde{n}^{(i)}(\mathbf{r}) \otimes h_{iwf}^{(i)}(\mathbf{r})\,. \tag{2.25}$$

Expression (2.24) can be proved to be the same as Eq. (2.17), but it is computationally more economical.

C. Estimation of Projection Variance When Each Projection in a Set Has Close Neighbors: Real-Space Comparison

For the general projection geometry, we have derived the 3-D variance estimate by estimating the projection noise through comparison among all projections, with the corresponding computations being necessarily demanding. If, in a projection set (e.g., a random-conical tilt series with a large number of projections), each projection has at least one neighbor directionally close enough so that variations among neighbor projections are mainly attributable to noise, we can borrow the neighbor projections in their entireties for the projection-noise estimation (Fig. 2). The corresponding 3-D variance estimate, which can be regarded as a special case of that found above, is easy to compute.

If the neighbors of projection i are projections $i-\delta$ to $i+\delta$, the estimate of the projection average is

$$\bar{s}^{(i)}(k,l) = \frac{1}{2\delta+1}\sum_{j=i-\delta}^{i+\delta} p^{(i)}(k,l)\,, \tag{2.26}$$

where $\delta = 1/2, 1, 3/2, 2, \ldots$, and the implied rule is that the absolutes of $j = i-\delta$ and $j = i+\delta$ are rounded to the next higher integer when δ is a half-integer. The projection-noise estimate is therefore

$$\tilde{n}^{(i)}(k,l) = \left(\frac{2\delta+1}{2\delta}\right)^{1/2}[p^{(i)}(k,l) - \bar{s}^{(i)}(k,l)]\,. \tag{2.27}$$

Corresponding to Eq. (2.8), the 3-D variance estimate is established by the backprojection of all variance components with

$$\begin{aligned}\tilde{\nu}_{wf}^{(i)}(\mathbf{r}) &= [\tilde{n}_{wf}^{(i)}(\mathbf{r})]^2\\ &= [\tilde{n}^{(i)}(k,l)\otimes h_{iwf}^{(i)}(\mathbf{r})]^2.\end{aligned} \tag{2.28}$$

D. Estimation of Projection Variance by Comparison of Projections and Reprojections of the Reconstruction

For the general projection geometry, the projection noise can also be estimated by the comparison of the projections and the corresponding reprojections of the reconstruction computed from the same projection data set.

For the purpose of the reprojection, we have to define the volume that fully contains the reconstructed object by an appropriate binary mask function $M(\mathbf{R})$. From Eq. (2.3), the masked reconstruction is

$$b_m(\mathbf{R}) \equiv \left\{\sum_{i=1}^{N} \mathrm{BP}[\,p_{wf}^{(i)}(\mathbf{r})]\right\} M(\mathbf{R})\,. \tag{2.29}$$

The reprojection of $b_m(\mathbf{R})$ at the view angle of projection i is

$$b^{(i)}(\mathbf{r}) \equiv \mathrm{PJ}_i[b_m(\mathbf{R})]\,. \tag{2.30}$$

So the filtered projection-noise estimate can be given as

$$\tilde{n}_{wf}^{(i)}(\mathbf{r}) = p_{wf}^{(i)}(\mathbf{r}) - b^{(i)}(\mathbf{r})\,. \tag{2.31}$$

This provides the 3-D variance estimate following Eqs. (2.8) and (2.9).

The estimate of Eq. (2.31) assumes that the statistical average of the reprojection should equal that of the filtered projection. In other words, the signal component of $p_{wf}^{(i)}(\mathbf{r})$ should be faithfully given by $b^{(i)}(\mathbf{r})$ so that their difference is due to the noise only. This assumption is

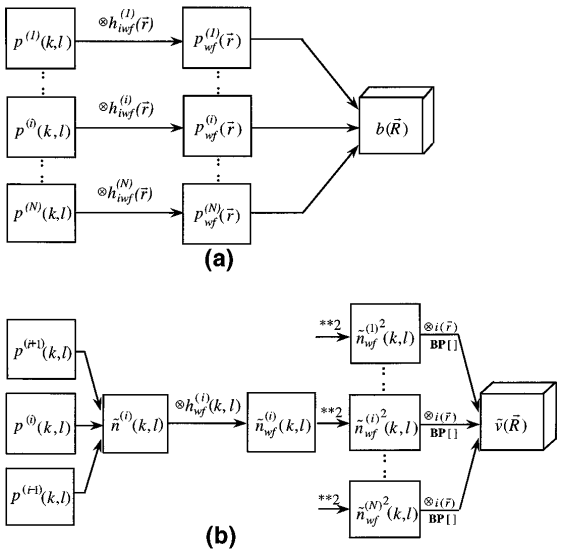

Fig. 2. Flow diagrams of reconstruction and corresponding variance. (a) Weighted backprojection reconstruction. The weighting and filtering operations are applied to projections first, and the reconstruction is obtained by summation of the weighted and filtered projections. (b) Variance estimation based on close neighbor comparisons. In the case shown, $\delta = 1$.

approximately fulfilled, provided that the boundaries of the 3-D mask function are generously chosen so as not to mask out the signal component.

Because $b^{(i)}(\mathbf{r})$ contains a noise component, the estimate provided by Eq. (2.31) is biased. [An unbiased version would require knowledge of both the variance of $b^{(i)}(\mathbf{r})$ and its 2-D covariance with $p_{wf}^{(i)}(\mathbf{r})$, which is practically not obtainable.] However, this bias decreases with an increasing redundancy of projections. By contrast, the other two estimates do not have this bias problem. On the other hand, these two estimates are affected by errors that are due to signal component differences, which are also reduced by high redundancy. Thus, in a nutshell, all three estimates require high redundancy of projections for good performance, although for different reasons. Because the bias is independent of the projection SNR, whereas the error that is due to the signal component difference is proportional to this SNR [see Appendix 1, relation (A20)], a low SNR, such as in low-dose micrographs, would favor the first two estimates.

E. Efficiency of Three-Dimensional Estimates

The 3-D variance estimate will be unbiased when it is derived from unbiased projection-noise estimates. However, a good estimator should be not only unbiased but also reliable (i.e., statistically efficient). The efficiency can be analyzed through the estimation of the variance of the 3-D variance estimate.

As shown in expression (2.16), the 3-D variance estimate is obtained by the summation of projection variance estimates $\tilde{\nu}_{wf}^{(i)}(\mathbf{r})$. For any two given projections j and k, their variance estimates $\tilde{\nu}_{wf}^{(j)}(\mathbf{r})$ and $\tilde{\nu}_{wf}^{(k)}(\mathbf{r})$ will be statistically dependent if a common projection is used in the estimation. This means that for the real-space approach of Subsection 2.C, the statistical dependence occurs between the variance estimates of neighbor projections, whereas for the Fourier-space approach of Subsection 2.B, such dependence can occur between the variance estimates of any two projections.

For the 3-D variance estimate $\tilde{\nu}(\mathbf{R})$, let us define the corresponding ideal 3-D variance estimate $\tilde{\nu}_0(\mathbf{R})$ as having the same expression but with $\tilde{\nu}_{wf}^{(i)}(\mathbf{r})$ being regarded as independent of i. Then we define an efficiency coefficient of the 3-D variance estimate as

$$\eta = \frac{\mathrm{var}[\tilde{\nu}_0(\mathbf{R})]}{\mathrm{var}[\tilde{\nu}(\mathbf{R})]}. \tag{2.32}$$

Because of the above-mentioned statistical dependence, the estimate $\tilde{\nu}(\mathbf{R})$ is statistically less reliable than the ideal estimate $\tilde{\nu}_0(\mathbf{R})$, and this makes $\eta < 1$. A good estimate should have a high efficiency coefficient (as close to 1 as possible).

With the assumption that the projection noise $n_{wf}^{(i)}(\mathbf{r})$ is Gaussian and that all projections have the same noise level, it can be shown that, for the 3-D variance estimate derived from Eq. (2.28), which corresponds to the real-space approach,

$$\eta|_{\delta=1/2} = \frac{2}{3}, \tag{2.33}$$

$$\eta|_{\delta=1} = 0.514, \tag{2.34}$$

where $\delta = 1/2$ and $\delta = 1$, which indicates that one or two neighboring projections are used in estimating the noise of a projection, respectively.

For the Fourier-space approach, the variation of the corresponding projection variance estimate in Eq. (2.24) is mainly due to the first term, which is a squared noise estimate [as is Eq. (2.28)]. Furthermore, the correlation between the variance estimates of different projections, which is due to the correlation between corresponding spectral-noise estimates, is expected to be similar to that of Eq. (2.28). So the corresponding 3-D variance estimate of Eq. (2.16) has an efficiency of between 0.5 and 1, depending on the projection orientations in the set [the detailed derivation can be given in a similar way to that for Eq. (2.28)]. The efficiency of Eq. (2.31) is difficult to estimate, but a range between 0.5 and 1 is also expected.

Through the 3-D variance analysis, we have presented different ways of searching for efficient estimators. For complicated situations, it is not always obvious whether an efficient estimation is possible, and there is no general rule for constructing one. Physical insights are often needed to identify the information sources and to express them optimally.

F. Covariance and Its Relationship with the Three-Dimensional Point-Spread Function

So far the focus has been on the 3-D variance. We should recall that the complete description of the statistics of a 3-D structure is given by the joint probability density function of all its voxels. In particular, this density function can be determined by the variance–covariance matrix of all the voxels if the noise of each voxel is Gaussian distributed.

The 3-D covariance estimation can be developed in parallel with the above 3-D variance estimation: for a given pair of voxels at $\mathbf{R}_1$ and $\mathbf{R}_2$,

$$\begin{aligned} c(\mathbf{R}_1, \mathbf{R}_2) &\equiv \overline{[b(\mathbf{R}_1) - \overline{b(\mathbf{R}_1)}][b(\mathbf{R}_2) - \overline{b(\mathbf{R}_2)}]} \\ &= \overline{\left\{\sum_{i=1}^{N} \mathrm{BP}[n_{wf}^{(i)}(\mathbf{r}_1)]\right\}\left\{\sum_{i=1}^{N} \mathrm{BP}[n_{wf}^{(i)}(\mathbf{r}_2)]\right\}} \\ &= \overline{\sum_{j=1}^{N} \mathrm{BP}[n_{wf}^{(i)}(\mathbf{r}_1)] \sum_{j=1}^{N} \mathrm{BP}[n_{wf}^{(i)}(\mathbf{r}_2)]} \\ &= \sum_{i=1}^{N}\sum_{j=1}^{N} \mathrm{BP}[c_{wf}^{(i)}(\mathbf{r}_1, \mathbf{r}_2)], \end{aligned} \tag{2.35}$$

where

$$c_{wf}^{(i)}(\mathbf{r}_1, \mathbf{r}_2) \equiv \overline{n_{wf}^{(i)}(\mathbf{r}_1) n_{wf}^{(i)}(\mathbf{r}_2)}. \tag{2.36}$$

Hence the covariance between two voxels can be estimated by the estimation of the projection covariances. The latter can be derived in three ways, parallel to the three approaches in estimating the projection variances in Subsections 2.B–2.D.

We now derive the relationship between the 3-D PSF and the 3-D covariance when the projection noise is independent between the pixels. The result will be important for the significance assessment of local features in a companion paper.[30]

Let us first define the PSF of a reconstruction. We consider an object that is made of a single point, so that

$p^{(i)}(k, l) = \delta(k, l)$. If this point object is substituted into Eqs. (2.4) and (2.3), the resulting reconstruction will be defined as a PSF:

$$h(\mathbf{R}) = \sum_{i=1}^{N} \mathrm{BP}[h_{iwf}^{(i)}(\mathbf{r})]. \tag{2.37}$$

A conical tilt series is collected with the specimen plane tilted by an angle ϑ_0. The projection central sections cover the 3-D Fourier space except a missing cone of the opening angle $90° - \vartheta_0$. The missing cone causes a resolution deterioration in the Z direction, which can be expressed by an elongation factor[21,22]:

$$\epsilon = \left(\frac{3 - \sin^2 \vartheta_0}{2 \sin^2 \vartheta_0} \right)^{1/2}. \tag{2.38}$$

With a low-pass filter $F(\mathbf{U})$ of the cutoff frequency U_f, the corresponding PSF has an elliptical-shaped central region of high density, with dimensions of $2/U_f$ in the $X-Y$ direction and $2\epsilon/U_f$ in the Z direction.

Now we consider an object $o(\mathbf{R})$ whose projections are represented as $o^{(i)}(\mathbf{r})$. An ideal measurement from an ideal instrument yields the average projection $\overline{p^{(i)}(k, l)} = o^{(i)}(k, l)$. If Shannon's sampling rate is satisfied so that $\mathrm{FT}[\overline{p^{(i)}(k, l)}] = o^{(i)}(\mathbf{r})$, the Fourier transform of Eq. (2.3) will give

$$\begin{aligned} S(\mathbf{U}) &= \overline{B(\mathbf{U})} \\ &= \sum_{i=1}^{N} \{\mathrm{FT}[\overline{p^{(i)}(k, l)}]\} H_{iwf}^{(i)}(\mathbf{u}) \\ &= \sum_{i=1}^{N} O^{(i)}(\mathbf{u}) H_{iwf}^{(i)}(\mathbf{u}) \\ &= O(\mathbf{U}) \sum_{i=1}^{N} H_{iwf}^{(i)}(\mathbf{u}) \\ &= O(\mathbf{U}) H(\mathbf{U}). \end{aligned} \tag{2.39}$$

Its inverse Fourier transform is

$$s(\mathbf{R}) = o(\mathbf{R}) \otimes h(\mathbf{R}); \tag{2.40}$$

hence the average reconstruction equals the object convoluted with the PSF.

If the projection density $\gg 1$ in the Fourier region outside the missing cone and below the cutoff frequency U_f, a successful weighted backprojection reconstruction should make $S(\mathbf{U}) = O(\mathbf{U})$ in this region, whereas $S(\mathbf{U}) \approx 0$ within the missing cone. From Eq. (2.39), this means that

$$\begin{aligned} H(\mathbf{U}) &\approx \begin{cases} 1 & \text{outside missing cone and } |\mathbf{R}| < U_f \\ 0 & \text{within missing cone and } |\mathbf{R}| > U_f \end{cases} \\ &\approx \begin{cases} F(\mathbf{U}) & \text{outside missing cone} \\ 0 & \text{within missing cone} \end{cases} \\ &\equiv F_0(\mathbf{U}). \end{aligned} \tag{2.41}$$

The approximation in the first step of approximation (2.41) is due to the fact that there is actually a region of transition from 1 to 0 at the missing cone boundary. In approximation (2.41), the PSF of the weighted backprojection reconstruction is roughly the PSF associated with low-pass filtration in which, additionally, the missing cone region is removed.

Now, if we make the specific assumption that the projection-noise component $n^{(i)}(k, l)$ is independent among the pixels $\mathbf{r}_{kl} = (k, l)$, the 3-D covariance of Eq. (2.35) can be expressed as a function of projection variances:

$$\begin{aligned} c(\mathbf{R}, \mathbf{R}_0) &= \sum_{i=1}^{N} \mathrm{BP}[\overline{\tilde{n}_{wf}^{(i)}(\mathbf{r}) \tilde{n}_{wf}^{(i)}(\mathbf{r}_0)}] \\ &= \sum_{i=1}^{N} \mathrm{BP}\left\{ \sum_{k,l} [\overline{n^{(i)}(\mathbf{r}_{kl})}]^2 h_{iwf}^{(i)}(\mathbf{r} - \mathbf{r}_{kl}) \right. \\ &\quad \left. \times h_{iwf}^{(i)}(\mathbf{r}_0 - \mathbf{r}_{kl}) \right\}. \end{aligned} \tag{2.42}$$

If it is further assumed that all projections have the same noise level, so that $\overline{[n^{(i)}(\mathbf{r}_{kl})]^2} = \nu_0$, Eq. (2.35) becomes

$$\begin{aligned} &c(\mathbf{R}, \mathbf{R}_0) \\ &= \nu_0 \sum_{i=1}^{N} \mathrm{BP}\left[\sum_{k,l} h_{iwf}^{(i)}(\mathbf{r} - \mathbf{r}_{kl}) h_{iwf}^{(i)}(\mathbf{r}_0 - \mathbf{r}_{kl}) \right] \\ &\approx \nu_0 \sum_{i=1}^{N} \mathrm{BP}\left[\iint h_{iwf}^{(i)}(\mathbf{r} - \mathbf{r}') h_{iwf}^{(i)}(\mathbf{r}_0 - \mathbf{r}'') \mathrm{d}^2\mathbf{r}' \mathrm{d}^2\mathbf{r}'' \right] \\ &= \nu_0 \sum_{i=1}^{N} \mathrm{BP}[h_{iwf}^{(i)}(\mathbf{r}_1) h_{iwf}^{(i)}(\mathbf{r}_1)] \Big|_{\mathbf{r}_1 = \mathbf{r} - \mathbf{r}_0}, \end{aligned} \tag{2.43}$$

that is, in Fourier space ($\mathbf{U}_1 = \mathbf{U} - \mathbf{U}_0$),

$$\begin{aligned} C(\mathbf{U}_1) &\approx \nu_0 \sum_{i=1}^{N} {H_{iwf}^{(i)}}^2(\mathbf{u}_1) \\ &= \nu_0 \left[\sum_{i=1}^{N} H_{iwf}^{(i)}(\mathbf{u}_1) \right] \left[\sum_{i=1}^{N} H_{iwf}^{(i)}(\mathbf{u}_1) \right] \\ &= \nu_0 H^2(\mathbf{U}_1) \\ &\approx \nu_0 H(\mathbf{U}_1), \end{aligned} \tag{2.44}$$

where the last step is due to the low-pass filter nature of the PSF [i.e., $H(\mathbf{U}_1)$ is roughly either 1 or 0; see relation (2.41)].

So if the projection noise is independent among the pixels and if its level is the same for all pixels of all projections, the 3-D covariance will have roughly the same pattern as the 3-D PSF.

3. THREE-DIMENSIONAL CONFORMATIONAL CHANGES

In Section 2, we have established the foundation for estimating the type-I variance, which determines the statistical significance of the reconstruction. We first analyze the feasibility of estimating the type-II variance and then develop the relationship between the two types of variance with the particle's conformational changes.

A. Single-Exposure Data Sets Do Not Allow Estimation of Type-II Variance

If, in a given data set, the 2-D projections contain sufficient structural information so that they can be partitioned according to the 3-D particle conformational states, then a reconstruction of each conformational state could

be computed, provided there are a sufficient number of projections for each partitioned subset. The differences among these reconstructions would yield the statistics about the structural variations of the particles, as defined by the type-II variance. In the case in which a tilt series of each particle is measured (by the use of multiple exposures), such partitioning is readily available from the data collection. However, from information within the projections alone, the partitioning could not be practically achieved because of the degenerative nature of the projecting process.

We raise an interesting and important question: can the type-II variance still be derived if the projections in a data set cannot be partitioned? This situation occurs with a single-exposure random-conical tilt data set in which only one projection of each particle is available from each view angle.

To answer this question, we make the simplifying and most favorable assumption that the projection noise comes only from the conformational changes.

Let $o^{(i)}(\mathbf{R})$ represent the conformation of particle i. Only one projection of certain view angle $p^{(i)}(\mathbf{r})$ can be collected from $o^{(i)}(\mathbf{R})$:

$$p^{(i)}(\mathbf{r}) = \mathrm{PJ}_i[o^{(i)}(\mathbf{R})]. \tag{3.1}$$

The full noise statistics of a function can be uniquely represented in both real and Fourier space; that is, the joint density function of $o(\mathbf{R})$ can be uniquely derived from that of $O(\mathbf{U})$ and vice versa. Specifically, the variance of $o(\mathbf{R})$ is determined from the covariance in Fourier space:

$$\begin{aligned}\mathrm{var}[o(\mathbf{R})] &\equiv \overline{[o(\mathbf{R}) - \overline{o(\mathbf{R})}]^2} \\ &= \iint \mathrm{cov}[O(\mathbf{U}_1), O(\mathbf{U}_2)] \\ &\quad \times \exp[i2\pi\mathbf{R}\cdot(\mathbf{U}_1 + \mathbf{U}_2)]\mathrm{d}^3\mathbf{U}_1\mathrm{d}^3\mathbf{U}_2 . \end{aligned} \tag{3.2}$$

If two Fourier points $\mathbf{U}_1$ and $\mathbf{U}_2$ are located on or close to the central section of an existing projection i, then it follows from Eq. (2.13) that the Fourier covariance between $\mathbf{U}_1$ and $\mathbf{U}_2$ is

$$\mathrm{cov}[O(\mathbf{U}_1), O(\mathbf{U}_2)] = C^{(i)}(\mathbf{U}_1, \mathbf{U}_2), \tag{3.3}$$

which can be estimated as shown in Subsection 2.B.

But if no projection central section can be found to contain both $\mathbf{U}_1$ and $\mathbf{U}_2$, their Fourier covariance cannot be estimated. This is because the projections are independent of each other, and no correlation information can be provided by projections each of whose central sections contains only one of the two points.

Hence, for the computation of type-II variance, the Fourier covariance between all Fourier-point pairs is needed. We note that any pair of points $\mathbf{U}_1$ and $\mathbf{U}_2$, along with the Fourier origin, determine a central section. This means that the estimation of type-II variance would require the availability of projections from all directions. Except for data collections that reley on totally random orientations of the molecule and cover the angular space sufficiently evenly,[31,32] there is no data-collection scheme that could meet this stringent requirement; we note that in the random-conical scheme the projection directions run along a single cone only. Similarly, if the Fourier plane determined by three Fourier points does not go through the Fourier origin, the joint statistics of these three points cannot be obtained at all.

This analysis shows that if, in a given projection data set, the projections cannot be classified to the particle conformational state it belongs to, the full particle statistics (described by the joint probability density function of all the points the particle occupies), including the variance of the 3-D particle, cannot be derived from projection statistics, even if the projection noise originates only from particle conformational changes. This is so for the single-exposure random-conical tilt series because the information about which particle a projection corresponds to is lost in the data-collection process. Hence our inability to partition the data results in the inability to estimate the type-II variance.

B. Three-Dimensional Variance of Two Varying Three-Dimensional Point Features

It was shown above that the full information of particle conformational change, including type-II variance, cannot be obtained from the single-exposure random-conical tilt series. But because a substantial portion of the type-I variance originates from the variations of particle structures (see Subsection 1.C), the variance should contain information about conformational changes that may be sufficient for answering some practical questions (such as whether a portion of the structure is moving) when combined with prior knowledge about the structure.

For the purpose of the analysis below we distinguish two categories of noise: one that is due to conformational changes and the other that is related to the measurement process (including preparation). We provide a simplified model of conformational change: the object is realized with two varying correlated point sources n_A and n_B at $\mathbf{R}_A$ and $\mathbf{R}_B$:

$$\mathrm{var}(n_A) = \mathrm{var}(n_B) = \nu_c , \tag{3.4}$$

$$\mathrm{cov}[n_A, n_B] = \gamma\nu_c , \tag{3.5}$$

where γ is the correlation coefficient. The two points could correspond to two positions assumed by a flexible molecule component ($\gamma < 0$) or to two ligand-binding sites ($-1 \le \gamma \le 1$).

Let $\mathbf{r}_A^{(i)}$ and $\mathbf{r}_B^{(i)}$ represent the points on projection i that are projected from $\mathbf{R}_A$ and $\mathbf{R}_B$, respectively. The projection noise can be expressed by

$$n^{(i)}(\mathbf{r}) = n'^{(i)}(\mathbf{r}) + n_A\delta[\mathbf{r}^{(i)} - \mathbf{r}_A^{(i)}] + n_B\delta[\mathbf{r}^{(i)} - \mathbf{r}_B^{(i)}], \tag{3.6}$$

where $n'^{(i)}(\mathbf{r})$ is the noise component from nonconformational changes. From the fact that $n^{(i)}(\mathbf{r})$ is independent with respect to i,

$$\begin{aligned}\nu(\mathbf{R}) &= \sum_{i=1}^{N} \mathrm{BP}[\overline{n_{wf}^{(i)2}(\mathbf{r})}] \\ &= \nu'(\mathbf{R}) + \nu_c{}^2[\mathrm{VPSF}(\mathbf{R} - \mathbf{R}_A) + \mathrm{VPSF}(\mathbf{R} - \mathbf{R}_A)] \\ &\quad + 2\gamma\nu_c{}^2\left(\sum_{i=1}^{N} \mathrm{BP}\{h_{iwf}^{(i)}[\mathbf{r} - \mathbf{r}_A^{(i)}]h_{iwf}^{(i)}[\mathbf{r} - \mathbf{r}_A^{(i)}]\}\right), \end{aligned} \tag{3.7}$$

where $h_{iwf}^{(i)}(\mathbf{r})$ is the PSF that expresses interpolation, weighting, and filtration, as defined by Eq. (2.5), and

VPSF is the 3-D variance PSF. The first term in Eq. (3.7) is the variance associated with noise that is due to nonconformational changes,

$$\nu'(\mathbf{R}) = \sum_{i=1}^{N} \mathrm{BP}[\overline{n_{wf}^{(i)2}(\mathbf{r})}], \tag{3.8}$$

and the second term contains two copies of the 3-D VPSF,

$$\mathrm{VPSF}(\mathbf{R}) = \sum_{i=1}^{N} \mathrm{BP}[h_{iwf}^{(i)2}(\mathbf{r})], \tag{3.9}$$

which corresponds to the 3-D variance of a single 3-D point noise source.

Most interestingly, the second term corresponds to two peaks at $\mathbf{R}_A$ and $\mathbf{R}_B$, reflecting the locations of the 3-D point sources of conformational changes. The third term (a cross term) is introduced by the correlation between the two points, as contributed by the backprojection of 2-D cross terms.

When $|\mathbf{R}_A - \mathbf{R}_B| > 2/U_f$ (where U_f is the filter cutoff frequency), then $|\mathbf{r}_A^{(i)} - \mathbf{r}_B^{(i)}| > 1/U_f$ for the majority of the projections. In this case, the corresponding 2-D cross terms will have projection-direction-dependent interference patterns, and their contributions to the 3-D cross term will be unfocused, in contrast to the coherent contributions of nonnegative 2-D functions to the 3-D VPSF terms. Hence the two VPSF peaks should stand out from the cross-term background. When $|\mathbf{R}_A - \mathbf{R}_B|$ becomes smaller ($< 2/U_f$), these two peaks will tend to merge into one. In either case, the 3-D variance map will reveal the existence of conformational changes. If the question is whether the particle contains a structural component that undergoes a change, the information derived from the observation of either one or two peaks is sufficient. But if we wish to know whether that change involves a relocation of a mass or a loss of a mass (e.g., ligand binding versus its absence), only the presence of two peaks could unambiguously point to the first case.

This analysis shows that the 3-D variance is indeed able to provide the locations of conformational changes.

4. CONCLUSIONS

Through systematic statistical analysis, a theory of estimating the variance distributions in 3-D reconstruction has been developed. The type-I variance, which indicates the reliability of the 3-D image, can be estimated through the estimation of the projection-noise distributions. Three different approaches to estimating the latter are proposed, pertaining to the special characteristics of a single-exposure random-conical tilt projection data set. By contrast, it was proved that the variance of the particle (type-II variance) cannot be estimated from such a data set. Furthermore, we have obtained the important result that the type-I variance can be used for the study of 3-D conformational changes.

It is worthwhile to step back to reflect where the 3-D variance analysis fits in the broad picture of structural analysis. The means toward the goal of obtaining 3-D structural information is parameter estimation, in which the parameters in our case are 3-D reconstruction and 3-D variance. The former, being a first-order moment, attempts to suppress the noise, whereas the latter, as a second-order moment, reflects some properties of the noise. Indeed there is no logical reason why we should stop our analysis at the level of the reconstruction when more information can be obtained from the data, in which our 3-D variance–covariance analysis is just one example of higher-order moment analysis.

In a subsequent paper,[30] we will show how the 3-D variance estimation theory can be employed in practice. The ways to use 3-D variance for assessing the significance of structural differences and of local features will be described. The application concerns the structural studies of a hemocyanin-Fab immunocomplex, in which local mass changes relate to the binding of a Fab fragment to four specific sites.

APPENDIX A: ESTIMATION OF ERROR THAT IS DUE TO SIGNAL COMPONENT DIFFERENCE OF NEIGHBOR PROJECTIONS

In the 3-D variance estimation in Section 2, we have ignored the signal component differences between neighboring projections in estimating the projection noise. We investigate the conditions under which the error in the 3-D variance estimate that is due to the signal component differences is sufficiently small. From a model analysis, we derive the upper bound of error from neighbor comparison as a function of projection redundancy and SNR.

When neighbor projections are used to estimate the noise of each projection, as shown in Subsection 2.C, the noise estimate $\tilde{n}^{(i)}(k, l)$ contains contributions from two independent sources: one is the true noise component $\tilde{n}_n^{(i)}(k, l)$ of neighbor projections that we hope is represented by $\tilde{n}^{(i)}(k, l)$, and the other is the difference of signal components $s^{(i)}(k, l) = \overline{p^{(i)}(k, l)}$ between neighbor projections, which causes errors in the projection-noise estimation of Eq. (2.11). We analyze the factors that affect the relative contribution of the projection signal component difference and the error this difference contributes to the 3-D variance estimate.

With

$$p^{(i)}(k, l) = s^{(i)}(k, l) + n^{(i)}(k, l), \tag{A1}$$

Eq. (2.27) becomes

$$\begin{aligned}\tilde{n}_{wf}^{(i)}(\mathbf{r}) &= \left(\frac{2\delta + 1}{2\delta}\right)^{1/2}\left[s_{wf}^{(i)}(\mathbf{r}) - \frac{1}{2\delta + 1}\sum_{j=i-\delta}^{i+\delta} s_{wf}^{(j)}(\mathbf{r})\right] \\ &\quad + \left(\frac{2\delta + 1}{2\delta}\right)^{1/2}\left[n_{wf}^{(i)}(\mathbf{r}) - \frac{1}{2\delta + 1}\sum_{j=i-\delta}^{i+\delta} n_{wf}^{(j)}(\mathbf{r})\right] \\ &= \tilde{n}_{wfn}^{(i)}(\mathbf{r}) + \tilde{n}_{wfs}^{(i)}(\mathbf{r}).\end{aligned} \tag{A2}$$

These two sources are independent; thus

$$\mathrm{var}[\tilde{n}_{wf}^{(i)}(\mathbf{r})] = \mathrm{var}[\tilde{n}_{wfn}^{(i)}(\mathbf{r})] + \mathrm{var}[\tilde{n}_{wfs}^{(i)}(\mathbf{r})]. \tag{A3}$$

This means that the difference of neighbor signal components always makes the noise level estimate larger and hence results in a larger 3-D variance estimate.

Two factors affect the relative contribution of signal component differences:

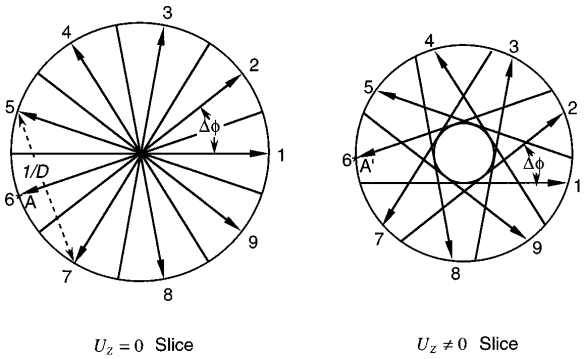

Fig. 3. Fourier projection geometry of a regular conical tilt series ($N = 9$) as indicated by two U_z slices. For a Fourier point A that is located in the central section plane of projection 6 and on the sphere surface where $|\mathbf{U}| = U_f$, the closest projections are 9 and 1 on the $U_z \neq 0$ slice, whereas they are 2 and 1 on the $U_z = 0$ slice. This shows that the projection density at a given Fourier point can be contributed by directionally remote projections. Also, note that the projection density is $m = 4$ and the neighbor projection density is $m' = 2$ at point A, which illustrates the relationship of $m = 2m'$ for a regular conical tilt series.

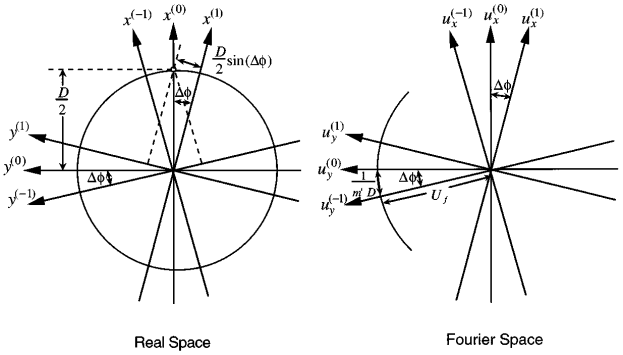

Fig. 4. Neighbor signal component difference when the object consists of a point at the periphery of a sphere with radius $D/2$. For explanation, see text.

(i) The SNR of the filtered and weighted projections. The signal level is defined by the image contrast. Normally the SNR is low for low-dose exposure [typically in the range of 1 after the low-pass filtration with a cutoff frequency of 1/(35 Å) for a specimen embedded in ice and a dose of ~ 10 electrons/Å].

(ii) Redundancy of projections. The more projections within a given angular interval, the more alike the neighbor signal components are. Practically only immediate neighbors are used (i.e., $\delta = 1/2$ or 1) in the projection-noise level estimation.

At this point, to describe the local redundancy in Fourier space, we introduce the concept of projection density $m(\mathbf{U})$, which is defined as the number of projections passing through a Fourier volume element of size $1/D^3$ located at $\mathbf{U}$. For the convenience of the discussion in this section, we refer to the projection density m as the average of $m(\mathbf{U})$ along a circle of radius U_f in the plane $\mathbf{U}_z = 0$.

Any two nonparallel projections will have a common line in 3-D Fourier space. It is important to realize that the projection density at a given point $\mathbf{U}$ can contain a contribution from directionally remote projections. For the analysis in this section, we introduce the neighbor projection density m', which is the redundancy when only neighbor projections are counted and directionally remote projections are excluded. As shown in Fig. 3, for a regular conical tilt series, the neighbor projection density is half that of the projection density:

$$m' = \frac{1}{2}\, m\,. \tag{A4}$$

The main difference between neighbor signal components arises from the peripheral part of the object's structure. The most drastic change is observed when we consider a point of magnitude S_0 at distance $D/2$ from the center of the object (let us put it on the X axis for convenience) and compare projections with directions that vary by small angles from the direction of the X axis:

$$o(\mathbf{R}) = S_0 \delta\left[\, \mathbf{R} - \left(\frac{D}{2}, 0, 0\right)\right]. \tag{A5}$$

With the projection direction in the $X-Y$ plane and the direction of projection 0 along the Y axis, as shown in Fig. 4,

$$\begin{aligned} s^{(i)}(\mathbf{r}) &= \mathrm{PJ}_i[o(\mathbf{R})] \\ &= S_0 d^{(i)}[\mathbf{r} - \mathbf{r}_0^{(i)}], \end{aligned} \tag{A6}$$

where

$$\mathbf{r}_0^{(i)} = \left[\, 0, -\frac{D}{2}\, \sin(\phi_i)\right]. \tag{A7}$$

In Fourier space, the weighted, filtered projection signal is

$$\begin{aligned} S_{wf}^{(i)}(\mathbf{u}) &= S^{(i)}(\mathbf{u}) W^{(i)}(\mathbf{u}) F^{(i)}(\mathbf{u}) \\ &= S_0 \exp[-i2\pi \mathbf{u} \cdot \mathbf{r}_0^{(i)}] W^{(i)}(\mathbf{u}) F^{(i)}(\mathbf{u})\,. \end{aligned} \tag{A8}$$

Now we apply a disk-shaped low-pass filtration function of radius U_f and the weighting function of a continuous conical tilt geometry, that is,

$$F^{(i)}(\mathbf{u}) = \begin{bmatrix} 1 & \text{when } |\mathbf{u}| \le U_f \\ 0 & \text{when } |\mathbf{u}| > U_f \end{bmatrix}, \tag{A9}$$

$$W^{(i)}(\mathbf{u}) = |u_y|\,. \tag{A10}$$

From the definition of neighbor projection density, we have (see Fig. 4)

$$U_f \Delta\phi = \frac{1}{m'D}\,, \tag{A11}$$

so

$$\frac{D}{2}\, \sin(\phi_j) = \frac{D}{2}\, \sin(\, j\Delta\phi) \approx \frac{D}{2}\, j\Delta\phi = \frac{j}{2m'U_f}\,. \tag{A12}$$

Now we choose immediate neighbors for noise estimation ($\delta = 1$). From Eqs. (A8) and (A10), it can be shown that

$$\begin{aligned} \tilde{N}_{wfs}^{(0)}(\mathbf{u}) &= \sqrt{\frac{3}{2}}\left[\, S_{wf}^{(0)}(\mathbf{u}) - \frac{1}{3} \sum_{j=-1}^{1} S_{wf}^{(j)}(\mathbf{u})\right] \\ &= \sqrt{\frac{2}{3}}\, S_0 \left[\, 1 - \cos\left(\frac{\pi u_y}{m'U_f}\right)\right] |u_y| F^{(i)}(\mathbf{u}) \\ &\ge 0\,. \end{aligned} \tag{A13}$$

So, in real space,

$$\begin{aligned}\tilde{n}^{(0)}_{wfs}(\mathbf{r}) &= \int \tilde{N}^{(0)}_{wfs}(\mathbf{u})\exp(-i2\pi\mathbf{u}\cdot\mathbf{r})\mathrm{d}^2\mathbf{u}\\ &= \int |\tilde{N}^{(0)}_{wfs}(\mathbf{u})\exp(-i2\pi\mathbf{u}\cdot\mathbf{r})|\mathrm{d}^2\mathbf{u}\\ &= \tilde{n}^{(0)}_{wfs}(0)\,. \end{aligned} \tag{A14}$$

Therefore,

$$\begin{aligned}&\max[\tilde{n}^{(0)}_{wfs}(\mathbf{r})]\\ &= \tilde{n}^{(0)}_{wfs}(0)\\ &= \int \sqrt{\frac{2}{3}}\,S_0\left[1-\cos\left(\frac{\pi u_y}{m' U_f}\right)\right]|u_y|F^{(i)}(\mathbf{u})\mathrm{d}^2\mathbf{u}\\ &= \sqrt{\frac{2}{3}}\,S_0 4\int_0^{U_f}\left[1-\cos\left(\frac{\pi u_y}{m' U_f}\right)\right]u_y({U_f}^2-{u_y}^2)^{1/2}\mathrm{d}u_y\\ \nu &= u_y/U_f\\ &= 4\sqrt{\frac{2}{3}}\,S_0{U_f}^3\int_0^1\left[1-\cos\left(\frac{\pi}{m'}\nu\right)\right]\nu(1-\nu^2)^{1/2}\mathrm{d}\nu\\ &= 4\sqrt{\frac{2}{3}}\,S_0{U_f}^3\int_0^1\left[\frac{1}{2}\left(\frac{\pi}{m'}\nu\right)^2\right.\\ &\quad\left.-\frac{1}{24}\left(\frac{\pi}{m'}\nu\right)^4+\ldots\right]\nu(1-\nu^2)^{1/2}\mathrm{d}\nu\\ &\approx \frac{4}{15}\sqrt{\frac{2}{3}}\,S_0{U_f}^3\left(\frac{\pi}{m'}\right)^2\left[1-\frac{1}{24}\left(\frac{\pi}{m'}\right)^2\right]. \end{aligned} \tag{A15}$$

Similarly

$$\begin{aligned}\max[s^{(0)}_{wf}(\mathbf{r})] &= s^{(0)}_{wf}(0)\\ &= \int S^{(0)}_{wf}(\mathbf{u})\mathrm{d}^2\mathbf{u}\\ &= 4S_0{U_f}^3\int_0^1 \nu(1-\nu^2)^{1/2}\mathrm{d}\nu\\ &= \frac{4}{3}\,S_0{U_f}^3\,, \end{aligned} \tag{A16}$$

so

$$\frac{\max[n^{(0)}_{wfs}(\mathbf{r})]}{\max[s^{(0)}_{wf}(\mathbf{r})]} \approx \frac{1}{5}\sqrt{\frac{2}{3}}\,S_0{U_f}^3\left(\frac{\pi}{m'}\right)^2\left[1-\frac{1}{21}\left(\frac{\pi}{m'}\right)^2\right]. \tag{A17}$$

Also,

$$\max[s^{(i)}_{wf}(\mathbf{r})] = \max[s^{(0)}_{wf}(\mathbf{r})]\,, \tag{A18}$$

$$\max[n^{(i)}_{wfs}(\mathbf{r})] \le \max[n^{(0)}_{wfs}(\mathbf{r})]. \tag{A19}$$

Therefore, for such a peripheral point, the relative error in the projection estimate, which is due to the signal component differences of neighbor projections, has an upper bound described by

$$\begin{aligned}\frac{\mathrm{var}[\tilde{n}^{(i)}_{wfs}(\mathbf{r})]}{\mathrm{var}[\tilde{n}^{(i)}_{wfn}(\mathbf{r})]} &\le \frac{\max[n^{(0)^2}_{wfs}(\mathbf{r})]\max[s^{(i)^2}_{wf}(\mathbf{r})]}{\max[s^{(i)^2}_{wf}(\mathbf{r})]\mathrm{var}[\tilde{n}^{(i)}_{wfn}(\mathbf{r})]}\\ &\approx \frac{2}{75}\,\frac{\pi^4}{m'^4}\left[1-\frac{1}{21}\left(\frac{\pi}{m'}\right)^2\right]^2 R_{\mathrm{sn}}\\ &\approx \frac{2.60}{m'^4}\,R_{\mathrm{sn}}\,, \end{aligned} \tag{A20}$$

where

$$R_{\mathrm{sn}} \equiv \frac{\max[s^{(i)^2}_{wf}(\mathbf{r})]}{\mathrm{var}[\tilde{n}^{(i)}_{wfn}(\mathbf{r})]}\,, \tag{A21}$$

which describes the SNR of a single projection after weighting and low-pass filtration.

For a typical micrograph with an exposure of 10 electrons/Å, $R_{\mathrm{sn}} = 1$ when a low-pass filtration of 1/(35 Å) is used. In this case, the maximum relative error from signal component differences is $\sim 2.60/m'$, which is 16.3% for $m' = 2$, 3.2% for $m' = 3$, and 1.0% for $m' = 4$.

We obtain the result that, for practical low-exposure experiments, a fivefold ($m = 5$) redundancy of projections can already make the relative contribution of the signal component differences between neighbor projections small enough for projection-noise estimations [for the 3-D variance estimate based on Fourier-space comparison in Subsection 2.B, a redundancy of $m = 3$ is good enough because the corresponding upper bound should be relation (A20) with m''s being replaced by m]. Because the 3-D variance is the sum of projection variances, the 3-D variance estimate has the same error range as the projection-noise level estimate because of the neighbor signal component differences.

The above conclusion is valid for features $D/2$ away from the center. If a point is at a distance R from the center, a substitution of $m'D/(2R)$ for m' into relation (20) gives the corresponding result, so the relative contribution of neighbor signal component differences, which correspond to the 3-D particle structure at R to the projection variance and hence 3-D variance, is $\propto R^4$. This means that it is mainly a margin close to the surface of the particle that leads to an appreciable fraction of the neighbor signal component difference. If a structure is globular, that is, if the rotational variation of the periphery structure is low, its neighbor projection signal component differences are expected to be small on average. The above discussion applies to the surface area of the particle and refers to the worst situation as far as neighbor signal component differences are concerned. In practice, however, the error can be much smaller than that predicted by relation (A20).

For a regular conical tilt geometry, the number of projections needed to satisfy Shannon's sampling rate, which corresponds to $m' = 1$, is given by[33]

$$N_0 = 2\pi D U_f \sin\vartheta_0 \qquad \text{for } N_0 \text{ even.} \tag{A22}$$

For a typical reconstruction with tilt angle $\vartheta_0 = 50°$, cutoff frequency $U_f = 1/(35$ Å), and practical particle diameter $D = 300$ Å, $N_0 = 41$. So $m' = 3$ will correspond to the number of projections $N = m'N_0 = 123$, and $m' = 4$ will correspond to $N = 164$, numbers that are well within the practical range of the number of projections used for a 3-D reconstruction.

ACKNOWLEDGMENTS

We gratefully acknowledge discussions with Pawel Penczek and Michael Radermacher. This work was supported by National Institutes of Health grants NIH 1

R01 GM 29169 and NIH 1 S10 RR0399801 to principal investigator J. Frank.

*Present address, ATS/WATCHER Division, KLA Instruments Corporation, 160 Rio Robles, P.O. Box 49055, San Jose, California 95161-9055.

REFERENCES

1. J. Radon, "Über die Bestimmung von Funktionen durch ihre Integralwerte längs gewisser Mannigfaltigkeiten. Berichte über die Verhandlungen der Königlich Sächsischen Gesellschaft der Wissenschaften zu Leipzig," Math. Phys. Klasse **69,** 262–277 (1917).
2. A. M. Cormack, "Representation of a function by its line integrals, with some radiological applications. I," J. Appl. Phys. **35,** 2908–2912 (1964).
3. D. J. DeRosier and A. Klug, "Reconstruction of three-dimensional structures from electron micrographs," Nature (London) **217,** 130–134 (1968).
4. P. W. Hawkes, "The electron microscope as a structure projector," in *Electron Tomography, Three-Dimensional Imaging with the Transmission Electron Microscope,* J. Frank, ed. (Plenum, New York, 1992), pp. 17–38.
5. R. A. Crowther, D. J. DeRosier, and A. Klug, "The reconstruction of a three-dimensional structure from its projections and its application to electron microscopy," Proc. R. Soc. London A **317,** 319–340 (1970).
6. R. Henderson and P. N. T. Unwin, "Three-dimensional model of purple membrane obtained by electron microscopy," Nature (London) **257,** 28–32 (1975).
7. J. Frank, B. F. McEwen, M. Radermacher, J. N. Turner, and C. L. Rieder, "Three-dimensional tomographic reconstruction in high voltage electron microscopy," J. Electron Tech. Microsc. **6,** 193–205 (1987).
8. W. Hoppe, J. Gassmann, N. Hunsmann, H. J. Schramm, and M. Sturm, "Three-dimensional reconstruction of individual negatively stained yeast fatty-acid synthetase molecules from tilt series in the electron microscopy," Hoppe-Seyler's Z. Physiol. Chem. **335,** 1483–1487 (1974).
9. J. Frank and W. Goldfarb, "Methods for averaging of single molecules and lattice-fragments," in *Electron Microscopy at Molecular Dimensions, State of the Art and Strategies for the Future,* W. Baumeister and W. Vogell, eds. (Springer-Verlag, New York, 1980), pp. 261–269.
10. M. Radermacher, T. Wagenknecht, A. Verschoor, and J. Frank, "Three-dimensional reconstruction from a single-exposure random conical tilt series applied to the 50S ribosomal subunit of *Escherichia coli,*" J. Microsc. (Oxford) **146,** 131–136 (1987).
11. M. Radermacher, T. Wagenknecht, A. Verschoor, and J. Frank, "Three-dimensional structure of the large subunit from *Escherichia coli,*" EMBO J. **6,** 1107–1114 (1987).
12. N. Boisset, J. C. Taveau, J. Lamy, T. Wagenknecht, M. Radermacher, and J. Frank, "Three-dimensional reconstruction of native *Androctonus australis* hemocyanin," J. Mol. Biol. **216,** 743–760 (1990).
13. T. Wagenknecht, R. Grassucci, J. Frank, A. Saito, M. Inui, and S. Fleisher, "Three-dimensional architecture of the calcium channel/foot structure of sarcoplasmic reticulum," Nature (London) **338,** 167–170 (1989).
14. J. Frank, P. Penczek, R. Grassucci, and S. Srivastava, "Three-dimensional reconstruction of the 70S *Escherichia coli* ribosome in ice: the distribution of ribosomal RNA," J. Cell Biol. **115,** 597–605 (1991).
15. P. Penczek, M. Radermacher, and J. Frank, "Three-dimensional reconstruction of single particles embedded in ice," Ultramicroscopy **40,** 33–53 (1992).
16. S. Srivastava, A. Verschoor, and J. Frank, "Eukaryotic initiation factor 3 does not prevent association through physical blockage of the ribosomal subunit–subunit interface," J. Mol. Biol. **226,** 301–304 (1992).
17. N. Boisset, M. Radermacher, R. Grassucci, J.-C. Taveau, W. Liu, J. Lamy, J. Frank, U. C. Taveau, and J. N. Lamy, "Three-dimensional immunoelectron microscopy of scorpion hemocyanin labeled with a monoclonal Fab fragment," J. Struct. Biol. **111,** 234–244 (1993).
18. N. Boisset, J.-C. Taveau, P. Penczek, J. N. Lamy, J. Frank, and J. Lamy, "Three-dimensional reconstruction of *Androctonus australis* hemocyanin labeled with a monoclonal Fab fragment," J. Struct. Biol. (to be published).
19. W. Liu, "3-D variance of weighted back-projection reconstruction and its application to the detection of 3-D particle conformational changes," in *Proceedings of the Forty-Ninth Annual Meeting of the Electron Microscopy Society of America* (San Francisco Press, San Francisco, 1991), pp. 542–543.
20. W. Liu, J. Frank, and N. Boisset, "An application protocol of 3-D variance estimation theory for significance assessment of reconstructions and detection of 3-D conformational changes," in *Proceedings of the Fiftieth Annual Meeting of the Electron Microscopy Society of America* (San Francisco Press, San Francisco, 1991), pp. 1064–1065.
21. M. Radermacher, "Three-dimensional reconstruction of single particles from random and nonrandom tilt series," J. Electron Microsc. Tech. **9,** 359–394 (1998).
22. J. Frank, "Classification of macromolecular assemblies studied as 'single particles'," Q. Rev. Biophys. **23,** 281–329 (1990).
23. J. L. Smith, W. A. Hendrickson, R. B. Honzatko, and S. Sheriff, "Structural heterogeneity in protein crystals," Biochemistry **25,** 5018–5027 (1986).
24. E. J. Hoffman and M. E. Phelps, "Positron emission tomography: principles and quantitation," in *Positron Emission Tomography and Autoradiography: Principles and Applications for the Brain and Heart,* M. Phelps and H. Schelbert, eds. (Raven, New York, 1986), pp. 237–286.
25. K. Wuthrich, *NMR of Proteins and Nucleic Acids* (Wiley, New York, 1986).
26. R. Ernst, G. Bodenhausen, and A. Wokaun, *Principles of Nuclear Magnetic Resonance in One and Two Dimensions* (Oxford Scientific, Oxford, 1990).
27. R. Hegerl and W. Hoppe, "Influence of electron noise on three-dimensional image reconstruction," Z. Naturforsch. **31a,** 1717–1721 (1976).
28. M. Radermacher, T. Wagenknecht, A. Verschoor, and J. Frank, "A new 3-D reconstruction scheme applied to the 50S ribosomal subunit of *E. coli,*" J. Microsc. **141,**PR1–RP2 (1986).
29. G. Harauz and M. van Heel, "Exact filters for general geometry three dimensional reconstruction," Optik **73,** 146–156 (1986).
30. W. Liu, N. Boisset, and J. Frank, "Estimation of variance distribution in three-dimensional reconstruction. II. Applications," J. Opt. Soc. Am. A **12,** 2628–2637 (1995).
31. M. Schatz, E. V. Orlova, P. Dube, J. Jäger, and M. van Meel, "Structure of *Lumbricus temestris* hemoglobin at 30 Å resolution determined using angular reconstitution," J. Struct. Biol. **114,** 28–40 (1995).
32. J. Frank, J. Zhu, P. Penzek, Y. Li, S. Srivastava, A. Verschoor, M. Radermacher, R. Grassucci, R. K. Lata, and R. K. Agrawal, "A model of protein synthesis based on cryo-electron microscopy of the *E. coli* ribosome," Nature (London) **376,** 441–444 (1995).
33. M. Radermacher and W. Hoppe, "Properties of 3-D reconstructions from projections by conical tilting compared to single axis tilting," in *Proceedings of the Seventh European Congress on Electron Microscopy* (Seventh European Congress on Electron Microscopy Foundation, Leiden, The Netherlands, 1980), Vol. 1, pp. 132–133.